journal

J. Am. Ceram. Soc., 76 [1] 166–72 (1993)

Evolution of Carbon during Burnout and Sintering of Tape-Cast Aluminum Nitride

Hongwen Yan*, W. Roger Cannon,* and Daniel J. Shanefield*

Department of Ceramic Engineering, Rutgers University, Piscataway, New Jersey 08855

The surface nature and the composition of AlN powder, as-received and exposed to binder burnout, were studied using XPS and TEM. The surface of as-received AlN powder was covered by a thin layer of aluminum oxynitride and oxide mixture. A small portion of residual carbon from binder burnout was bound to oxygen atoms on the AlN powder surface, and the majority of the carbon was amorphous graphitoid carbon which covered the AlN powder surface uniformly. AlN samples were made using tape casting and pressureless sintering. Surface-carbon-to-oxygen ratio of AlN powder after binder burnout was evaluated using XPS. The surface C/O atomic ratios were observed to correlate with the sintering behavior, the composition of the second phase, the second phases distribution, and grain-boundary composition, as well as thermal conductivity of AlN samples.

I. Introduction

ALUMINUM NITRIDE (AlN) has attracted much attention as a high-thermal-conductivity ceramic substrate. The theoretical thermal conductivity of single-crystalline AlN at room temperature is about 320 W/(m·K); however, the thermal conductivity of dense polycrystalline AlN is reduced significantly by impurities, especially by oxygen and carbon. Slack[1] pointed out that the thermal conductivity of AlN depends heavily on the oxygen impurity level when oxygen appears as a substitutional impurity within the AlN lattice. These oxygen impurities scatter phonons mostly from the mass defects caused by aluminum vacancies. Later publications have confirmed the detrimental effects of oxygen impurities on the thermal conductivity of AlN.

Besides oxygen, carbon is also believed to be an important impurity which affects the thermal conductivity of AlN, although the mechanism is not completely understood. Kurokawa *et al.*[2] found that adding 0.5 wt% of carbon increased thermal conductivity, but adding more than 1.0 wt% of carbon lowered the thermal conductivity significantly due to a decrease in sintered density. Horvath *et al.*[3] studied the effects of carbon on the sintering behavior of AlN and found that carbon, as an additive, directly enhances the grain-growth rate of AlN and retards the densification. Several researchers[4-6] have pointed out that a certain amount of carbon is needed to reduce the oxygen impurity level by carbon deoxidation, in which the free carbon reacts with the impurity oxygen, producing carbon monoxide gas. Recently, Lee[7] reported that 0.5% carbon with Y_2O_3 as combined sintering aids reduced the oxygen level in AlN powders, reduced the amount of the grain-boundary phase, and slowed down the grain growth of AlN. The use of the two sintering aids also changed the grain-boundary phase from aluminum-rich to yttrium-rich grain boundaries. Virkar *et al.*[8] proposed that the lower equilibrium activity of Al_2O_3 in the yttrium-rich second phase can cause a lower Al vacancy concentration in the AlN grains and thus improve the thermal conductivity.

The idea of microstructure alone having an effect on the thermal conductivity of polycrystalline AlN is debatable. Slack *et al.*[9] concluded that intrinsic grain-boundary scattering should have little or no effect on the thermal conductivity of AlN. Weisenbach *et al.*[10] concluded that the main contribution to the difference in thermal conductivity was the oxygen level in the AlN grain and not the microstructural difference. But Shinozaki *et al.*[11] found that, above 170 W/(m·K), the grain-boundary oxide phase was the primary determinant of thermal conductivity. Enloe *et al.*,[12] in studying $CaCO_3$-doped AlN, found that most residual oxygen stayed along the grain boundary, and thermal conductivity correlated with the effective grain-boundary thickness. Consequently, in these cases they concluded that grain boundaries dominated thermal conductivity in low-porosity AlN samples.

In the present work, AlN substrates were made by the tape-casting technique. Some residual carbon from binder burnout accompanies this technique. X-ray photoelectron spectroscopy (XPS) and high-resolution transmission electron microscopy (TEM) were used to study the chemical and physical nature of the residual carbon at the surface of AlN powder. The crystalline state of the AlN substrates after sintering was analyzed using XRD; microstructures of AlN samples were studied using TEM. Thermal conductivity was measured using the laser flash method. The effects of residual carbon on the thermal conductivity and microstructure of AlN were explored.

II. Experimental Procedure

(1) Processing

The aluminum nitride powder used was manufactured by Dow Chemical Co. and has a 3.1 m^2/g surface area. The supplier's chemical analysis indicates that it contains 1.07% oxygen, 0.16% carbon, and less than 300 ppm metal impurities. 3 wt% of Y_2O_3 was used as a sintering aid. The Y_2O_3, manufactured by Mitsubishi Kasei, is 99.9% pure, according to the supplier. The particle size of this Y_2O_3 powder is 0.8 μm.

Green sheets of the AlN substrates were prepared by tape casting. Slip formulations containing poly(vinyl butyral) (PVB, B-98, Monsanto, St. Louis, MO) binder and poly(propylene carbonate) (PPC, QPAC-40M, Air Products, Allentown, PA) binder were used because of the significant difference in their residual carbon contents. Table I shows the formulations for the tape-casting slips.

The thickness of the AlN tape was about 0.6 mm, and the green density after binder burnout was around 52% of theoretical density. Binder burnout was carried out at a heating rate of 5°C/min to 550°C in nitrogen atmosphere or to 500°C in air. Samples were placed on an AlN setter and sintered in a furnace with a tungsten heating element at 1800°C under slowly flowing nitrogen for 1 h.

A. V. Virkar—contributing editor

Manuscript No. 195842. Received March 31, 1992; approved August 28, 1992.
Supported by the Center for Ceramic Research at Rutgers University and the New Jersey State Commission on Science and Technology.
*Member, American Ceramic Society.

Table I. Tape Casting Formulation (vol%)

	7.0 vol% PVB	10.0 vol% PPC
AlN powder	30.0	30.0
MEK		27.0
EtOH	22.0	
Toluene	33.0	27.0
Phosphate ester (PS-21A)	0.1	0.1
Ethylene-imine polymer (KD-3)	1.0	
Oleate (fish oil)		1.0
Poly(ethylene) glycol	2.0	2.0
Dibutyl phthalate	2.0	2.0
Butyl benzyl phthalate	2.0	
Cyclohexanone	1.0	1.0

Table II. Weight Percent of Residual Carbon after Binder Pyrolysis at 600°C

	PVB	AlN/PVB	PPC	AlN/PPC
Air	0.0	0.3 to 0.5	0.0	0.1 to 0.3
Nitrogen	1.4 to 1.6	3.0 to 3.5	0.0	0.8 to 1.5

(2) Characterization of Residual Carbon at the Surface of AlN Powder

10 wt% binder and 90 wt% of AlN powder were mixed uniformly in an organic solvent. After drying, the mixture underwent a binder burnout process. X-ray photoelectron spectroscopy (XPS, XSAM-800, Kratos, Ramsey, NJ) was used to evaluate the amount of the residual carbon at the surface of the AlN powder and the binding state between the residual carbon and other elements at the surface of the AlN powder. A sample of AlN powder, as-received, and the AlN powders from AlN/binder mixtures for a variety of pyrolysis conditions were tightly packed into a shallow depression in an aluminum sample stub. The samples were then gradually degassed in the sample introduction chamber and placed into the ultrahigh vacuum (10^{-7} to 10^{-8} torr) chamber of the XPS spectrometer for examination. The electron signal was generated by nonmonochromatic Mg$K\alpha$ radiation produced from an Mg anode under 16 keV and 14 mA. The spectra were collected using a hemispherical electron energy analyzer with a bias setting of 5.0 eV. High-magnification and high-resolution scans over narrow energy ranges were recorded around each peak of interest (Al2p, N1s, O1s, and C1s) for 20 min to obtain surface chemical information.

The TEM sample was prepared using the dispersion method. AlN powder with residual carbon was dispersed into reagent-grade ethanol. A 3-mm copper grid with a discontinuous carbon film was dipped into the dilute dispersion for several seconds, followed by evaporation of the solvent. High-resolution microscopy (TEM, EM-002B, Topcon, Japan) was performed to observe and analyze the residual carbon at the AlN powder surface.

(3) Characterization of Sintered AlN Pellets

The bulk density of sintered AlN samples was measured using Archimede's method. X-ray diffractometry (XRD, Siemens D500, Madison, WI) was used to identify the second phases present in the AlN samples. The distribution of second phases was studied using transmission electron microscopy. Auger emission spectroscopy (AES, XSAM800 Kratos, Ramsey, NJ) was employed to examine the vacuum-fractured cross-section of AlN pellets. This procedure measured the grain-boundary chemistry composition because of the intergranular fracture surface.

Thermal diffusivity was measured by the laser-flash method using an Nd–glass laser. AlN pellets about 1.5 mm thick and 15 mm in diameter were polished down to 600 grit and then sputter-coated with a thin gold film to prevent direct transmission of the laser beam. A thin carbon coating on top of the thin gold film was applied to increase the absorptivity of the front face and the emissivity of the back face. Thermal conductivity was calculated according to the equation $K = D\rho C_p$, where D is thermal diffusivity, ρ is the density, and C_p is heat capacity of the specimens.

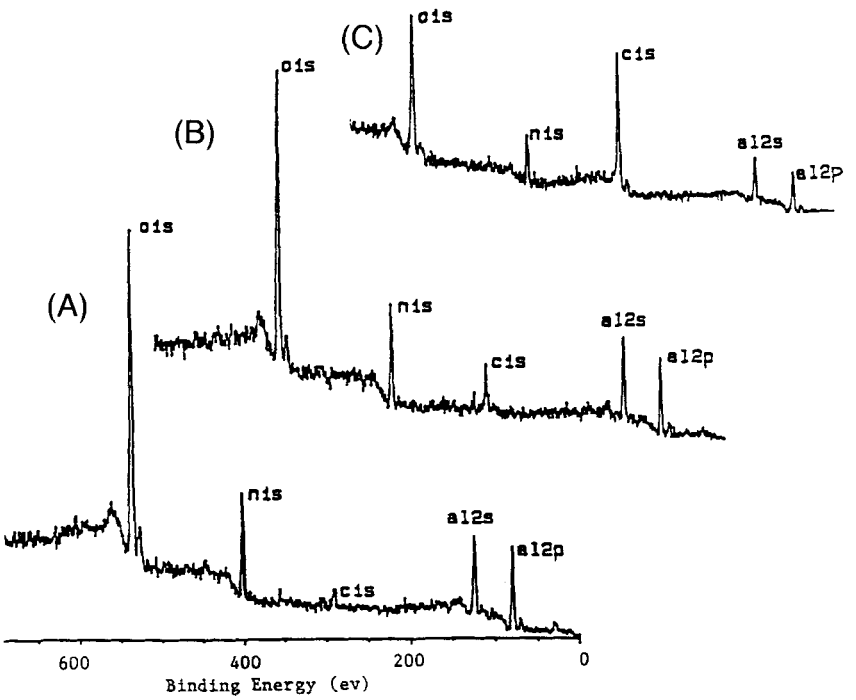

Fig. 1. XPS spectra of AlN Powder: (A) as-received; (B) powder after AlN/PVB mixture pyrolysis in air; (C) powder after AlN/PVB mixture pyrolysis in N_2.

Table III. Line Position and Surface Composition of AlN Powder from XPS

Powder	Line spectrum	Position (eV)	FWHM* (eV)	Concentration (at.%)	C/O
As-received AlN powder	Al2*p*	73.6	2.1	30.0	
	N1*s*	396.5	2.1	22.6	
	O1*s*	531.0	3.1	43.0	
	C1*s*	285.0	2.0	4.4	0.10
AlN/PVB binder burnout in air	Al2*p*	73.7	2.2	29.0	
	N1*s*	396.5	2.1	14.1	
	O1*s*	530.9	3.0	45.0	
	C1*s*	284.7	2.0	11.9	0.26
AlN/PVB binder burnout in nitrogen	Al2*p*	73.6	2.1	26.7	
	N1*s*	396.5	1.8	15.6	
	O1*s*	530.9	2.7	24.8	
	C1*s*	284.2	1.6	32.9	1.32
AlN/PPC binder burnout in air	Al2*p*	73.4	2.1	26.6	
	N1*s*	396.5	2.0	17.8	
	O1*s*	530.8	3.0	46.4	
	C1*s*	284.7	2.0	9.2	0.20
AlN/PPC binder burnout in nitrogen	Al2*p*	73.5	2.2	26.5	
	N1*s*	396.5	1.9	16.1	
	O1*s*	530.9	2.8	38.0	
	C1*s*	284.0	1.8	19.4	0.51

*Full width at half maximum.

III. Results and Discussion

(1) Carbon at the Surface of AlN Powder

Green sheets of AlN substrate made by tape casting were composed of AlN powder, a polymer binder, and other organic additives. Residual carbon in AlN tape after binder burnout originated primarily from the binder except with polycarbonate, where there was little residual carbon and the residue from the fish oil was significant. In this section, only AlN and binder mixtures were considered. AlN/PVB mixtures and AlN/PCC mixtures were subjected to the TGA examination in an air and a nitrogen atmosphere to 600°C at a rate of 5°C/min. Table II lists the weight percent of residual carbon after polymer binder pyrolysis, both in the pure polymer state and in the presence of AlN powder. The weight percent of residual carbon of the AlN mixture was based on the amount of polymer binder in the mixture. PPC burned out more cleanly than PVB did. PPC left no char to within the limits of detection even after the binder pyrolysis in a nitrogen atmosphere. More residual carbon was detected by TGA from the AlN/binder mixtures than from pure polymer binder. In previous studies concerning interaction between PVB binder and AlN powder during binder burnout,[13] residual carbon was adsorbed at the AlN powder surface by the interaction between volatile pyrolysis products and powder surface. This type of mechanism was referred to as "gas-phase-mediated char."[14] Most of the extra residual carbon detected from AlN/binder mixture was believed to form through this mechanism.

The X-ray photoelectron spectra of AlN powder, produced by scanning over a wide energy range (0 to 1 keV), are shown in Fig. 1, where (A) was from as-received AlN powder, (B) was from AlN powder after AlN/PVB mixture pyrolysis in air, and (C) was from AlN powder after AlN/PVB mixture pyrolysis in nitrogen atmosphere. Figure 1 shows that the major elements at the AlN powder surface were Al, N, O, and C. Since the AlN powder was manufactured using the carbothermal reduction method, the carbon in the as-received AlN powder was mostly in an isolated state, instead of adsorbed to the AlN powder surface, and in a much smaller concentration. A very weak carbon peak appeared in the XPS spectrum of as-received AlN powder. AlN powder from the AlN/PVB mixture after PVB pyrolysis in nitrogen showed a strong carbon peak in the X-ray photoelectron spectrum.

The high-resolution scan over the narrow energy range around Al2*p*, N1*s*, O1*s*, and C1*s* elements was performed to obtain information on the chemical environment and to give quantitative estimates of the surface elemental composition. The peak positions have been shifted by correcting for static charging of the sample. Correction positions were obtained by scanning the same sample with a trace of gold on top of the AlN samples. The position of Au4*f* at 84.0 eV was used for the internal position calibration. Table III lists the XPS results showing line positions, atomic concentration, and carbon-to-oxygen ratio.

The XPS signal of the Al2*p* photoelectrons for the as-received AlN powder clearly indicated a peak at 73.6 eV, which was believed to be due to the Al–N bond with contributions from Al–O bonding at the surface of the powder.[15,16] The line position of the N1*s* peak at 396.5 eV was due to Al–N bonding.[17] The fact that the N/Al ratio was less than unity suggested that all of the nitrogen ions were bonded to aluminum ions, while the excess aluminum ions were bonded to oxygen ions in either alumina or alumina oxynitride. The band widths at the half height of the O1*s* peak were much larger (3.0 eV) than that reported for Al_2O_3 (2.2 eV), and thus it is suggested that an aluminum oxynitride was present near the surface. However, since the oxygen content was the highest among these four elements, it is assumed that some Al_2O_3 was present also. Although the amount of this aluminum oxynitride cannot be evaluated from these XPS data, it is concluded that the surface of the powder was covered by a thin layer of a mixture of aluminum oxide and oxynitride, which is consistent with the results published by Ponthieu and co-workers.[18]

After the AlN/binder mixture underwent a binder burnout process, a layer of residual carbon was adsorbed onto the AlN powder surface. XPS data of these AlN powders in Table III show that the total amount of aluminum and nitrogen at the powder surface was reduced with increasing carbon, but the nitrogen-to-aluminum ratio was kept approximately the same. When the binder was burned out in air, the carbon concentration at the surface increased above that of the as-received powder. At the same time, the oxygen level increased also, which kept the carbon-to-oxygen ratio low, even though the carbon content was raised by a large amount. On the other hand, when binder was burned out in nitrogen atmosphere, the significant carbon concentration increase came with the decrease of the oxygen content, which made a high carbon-to-oxygen ratio. The peak position of Al2*p*, O1*s*, and N1*s* did not shift from the position of as-received powder, but the carbon peak showed an obvious shift.

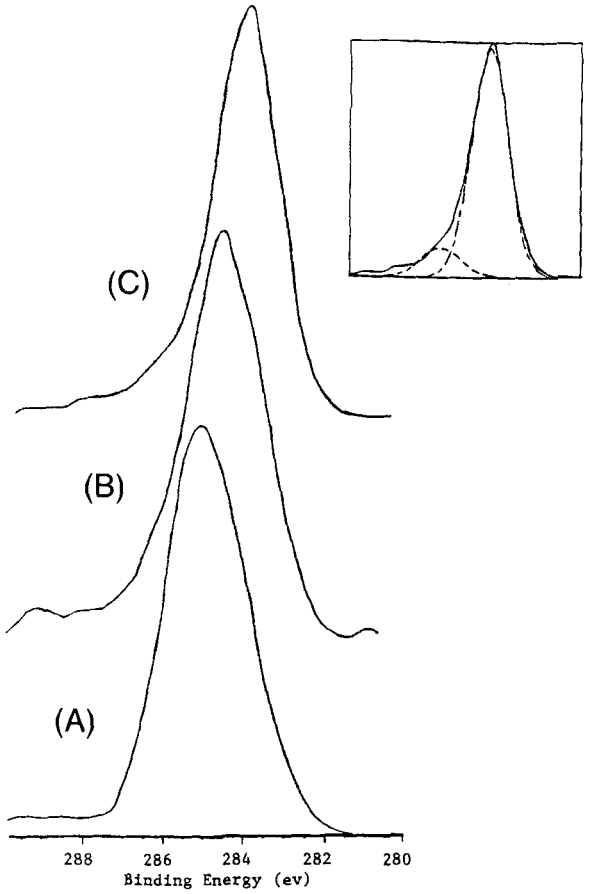

Fig. 2. XPS spectra of C1*s* photoelectrons: (A) as-received; (B) powder after AlN/PVB mixture pyrolysis in air; (C) powder after AlN/PVB mixture pyrolysis in N_2.

Figure 2 shows high-resolution and deconvoluted C1*s* XPS peaks from the as-received AlN powder, the AlN powder from the AlN/PVB mixture after binder burnout in air, and after binder burnout in nitrogen. The intensities of C1*s* peaks were normalized to the same height. It was observed that (1) the position of the C1*s* peak shifted towards lower binding energies for the AlN powder after binder burnout, and the higher the carbon content, the lower the binding energy; (2) the half-height band widths of the C1*s* peak decreased for the AlN powder after binder burnout, and the higher the carbon level, the narrower the band widths; (3) the C1*s* peak can be deconvoluted into two peaks, a small one with higher binding energy (286.0 eV) and a major one with lower binding energy (284.0 eV). The higher binding energy peak corresponded to the carbon which was bound to oxygen at the surface of AlN powder, while the peak at the lower binding energy arose most likely from graphitoid carbon which was formed by carbon binding to carbon itself. The AlN powder from the AlN/PPC mixture after binder burnout behaved the same as that from the AlN/PVB mixture, except that less carbon was adsorbed on the AlN powder surface and more oxygen was detected on the powder surface even when the binder was burned out in nitrogen atmosphere.

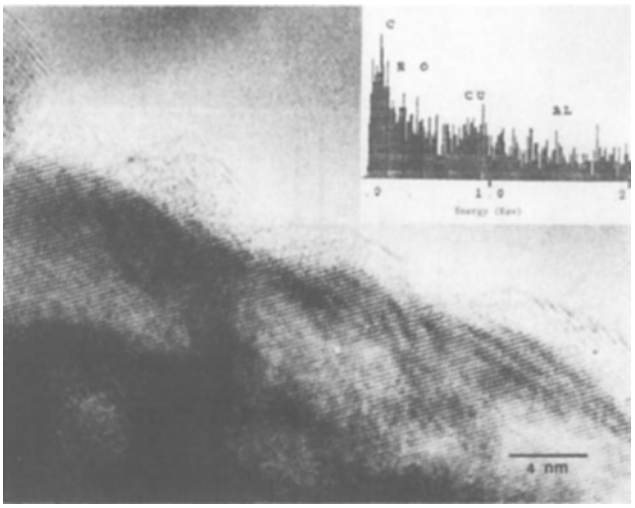

Fig. 3. High-resolution TEM picture of AlN powder with residual carbon.

Figure 3 shows a high-resolution micrograph of AlN powder with residual carbon adsorbed onto the powder surface. The clear lattice image was from the AlN lattice itself, and a clear amorphous layer was observed. The EDS spectrum attached to the TEM micrograph was taken from the amorphous cluster which indicated only a carbon peak.

From the above results it could be concluded that the surface of as-received AlN powder was covered with a layer of aluminum oxide and oxynitride mixture. The binder burnout process for the AlN/binder mixture left a significant amount of carbon residue on the AlN powder surface. The first layer of carbon is bound to oxygen atoms in the oxide and oxynitride layer at the surface, while additional carbon is bound to carbon itself, forming amorphous graphitoid carbon clusters which covered the powder surface uniformly.

(2) Effects of Residual Carbon on Microstructure and Thermal Conductivity of AlN

In order to study the effects of carbon residue on sintering and microstructure of AlN, the tape casting formulations in Table I were used. It was shown in another paper[13] that the plasticizer affects the total carbon residue; nevertheless, the nature of the carbon residue is likely not greatly changed, and most of this carbon residue is amorphous graphitoid carbon covering the AlN powder surface uniformly. Table IV lists some chemical and physical properties of AlN samples after sintering, and including the binder burnout conditions before sintering. The carbon and oxygen atomic concentrations at the AlN powder surface were evaluated by XPS after binder burnout and were not too far different from results of Table II for the powder/binder mixture alone.

AlN samples with PVB binder did not sinter when the binder was burned out in nitrogen atmosphere, where the C/O ratio was 1.51. In order to densify this sample, additional air treatment was applied to obtain a lower C/O atomic ratio. Since Y_2O_3 is thermodynamically more stable than Al_2O_3,[19] the carbon deoxidation during sintering occurred only between Al_2O_3 and C following this chemical reaction:

Table IV. Some Chemical and Physical Properties of AlN Samples

	Sample C	Sample D	Sample A	Sample B	Sample E
Binder	PVB	PVB	PPC	PPC	PVB
Burnout condition	Air 500°C, 1 h	N_2 550°C, 1 h	Air 500°C, 1 h	N_2 550°C, 1 h	N_2 550°C, 1 h; air 450°C, 0.5 h
At.% carbon*	14.5	36.3	13.1	26.8	25.5
At.% oxygen*	45.5	24.1	50.9	34.4	38.6
Bulk density (%)	98.0	80.0	99.0	99.0	99.0
Thermal conductivity (W/(m·K))	145		150	165	155
Second phase	$Al_2Y_4O_9$, $AlYO_3$	Y_2O_3	$AlYO_3$	$Al_2Y_4O_9$	$Al_2Y_4O_9$

*Surface composition. Data are normalized.

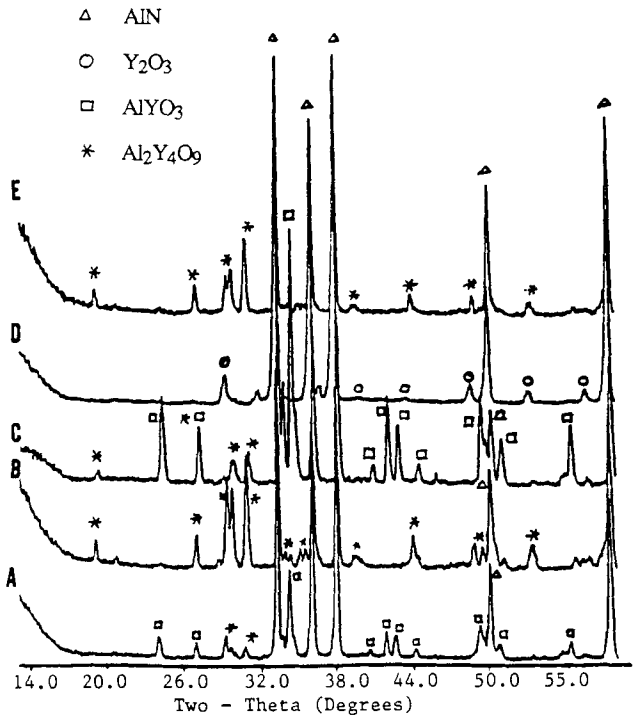

Fig. 4. X-ray diffraction pattern of AlN samples.

$$Al_2O_3 + 3C + N_2 \rightarrow 2AlN + 3CO \quad (1)$$

In order to remove all the oxygen, 3 mol of carbon should be used for 1 mol of aluminum oxide. If Al_2O_3 is essential to sintering, then the carbon-to-oxygen atomic ratio of C/O = 1.0 could be considered a threshold, and only the AlN samples with a C/O atomic ratio less than 1.0 could be sintered. Figure 4 presents the X-ray diffraction patterns for these samples. The sample with PVB binder burnout in nitrogen (C/O = 1.51) had only Y_2O_3 as a second phase. This inferred that all Al_2O_3 at the AlN powder surface had reacted with carbon, and no Al_2O_3 was left to form a liquid phase with the Y_2O_3, which was apparently necessary for densification of the AlN sample.

A quite good correlation between the surface carbon/oxygen ratio and the composition of the second phases was shown in Table IV. Figure 5 shows the correlation between the C/O atomic ratio at the AlN powder surface and the Al/Y ratio in the second phase of the sintered material, and also the thermal conductivity of AlN sintered pellets. Figure 5 indicates that (1) with the surface C/O ratio increasing, second phases in AlN substrates became yttrium-rich; (2) as the C/O ratio increased and the second phases became yttrium-rich, the thermal conductivity of the AlN substrate increased.

Sample PA (C/O = 0.32) (12 KX)

Sample QB (C/O = 0.78) (12 KX)

Fig. 6. TEM picture of AlN samples.

It had been found also that the distribution of second phases in the samples was different with different C/O ratios. Complete wetting is a requirement for liquid-phase sintering. Toward the end of the sintering process, the wetting ability of the liquid phase changed, which caused the liquid phase to migrate to the grain triple points. To further study the effects of

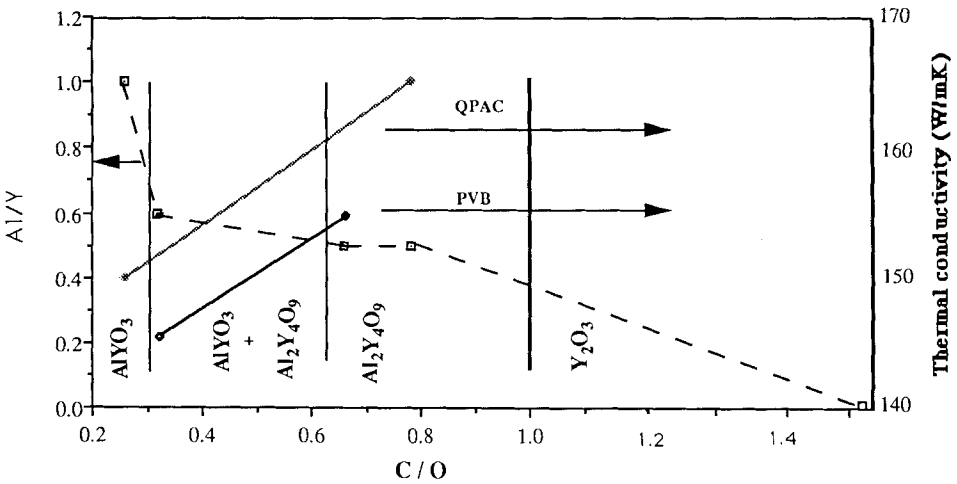

Fig. 5. Effects of C/O surface composition on Al/Y second phase and thermal conductivity.

the C/O ratio on the second phase, sample PA (PVB, binder burnout in air) whose C/O ratio was 0.32, and sample QB (PPC, binder burnout in nitrogen) whose C/O ratio was 0.78, were examined using transmission electron microscopy. Figure 6 shows the TEM micrograph of these two samples. The second-phase particles in the PA sample were widely distributed and of smaller size. The dihedral angles of these second-phase particles were around 60°. Some second-phase particles still remained at the grain boundaries. In comparison, the second-phase particles in sample QB were concentrated more on triple points and were larger. The dihedral angles of these second-phase particles were about 90°. It appeared that the liquid phase in the QB sample no longer wet the grain boundary at the end of the sintering process, and the second phase migrated to the triple points. Since the wetting ability was so poor, the liquid phases stayed together and formed larger second-phase particles. In the PA sample, the liquid phase still wet the grains at some level toward the end of the sintering, which left some second phase at the grain boundaries and made the second phase widely distributed and with smaller dihedral angles. Thus, the lower thermal conductivity of AlN samples with lower C/O ratio may be related to the second-phase distribution.

In order to further understand the effects of the surface C/O atomic ratio of AlN powder on the grain boundary composition after sintering, Auger emission spectroscopy (AES) was employed to examine the vacuum-fractured cross section of AlN pellets. Figure 7 presents the AES spectra of QA (PPC, binder burnout in air) and QB samples. The C/O ratio of QA sample was 0.26. Table V lists the chemical composition at the grain boundaries from the above spectra. Results indicate that there was no Y_2O_3 phase along the grain boundaries. There was, however, a clear carbon peak for the QB sample, which had a higher C/O ratio than the QA sample. The carbon peak in the QA sample was not above the noise level. Table IV shows that

Table V. Chemical Composition (at.%) at AlN Grain Boundary by AES

	Al	N	O	C
QA	41.6	36.7	21.7	Noise level
QB	40.2	37.4	12.6	9.8

the Al and N contents in both samples were similar, and only the O and C contents were significantly different between them. The oxygen level at grain boundaries correlated with the thermal conductivity reading. Fujimoto and Ueda[20] used CF_4 reactive gas reacting with O and Ca located at the grain boundaries to remove oxygen impurities and second phase at the grain boundaries in AlN ceramics. Thermal conductivity of the AlN sample increased from 180 to 230 W/(m·K) after 5-h gas treatment. Thus, the higher C/O ratio on the powder surface removed oxygen impurities from the grain boundaries, and alternatively this may be responsible for the increased thermal conductivity. Furthermore, the difference in grain-boundary composition may be useful in explaining the difference in wetting characteristics of the PA and QB samples.

Further research is being carried out to explore the oxygen and carbon content inside the AlN grain by EELS. In this study, intragranular carbon has been found occasionally in localized areas but did not appear to be in a second phase. It is hoped that these studies will further clarify the effect of microstructure and impurities on thermal conductivity.

IV. Conclusions

As-received AlN powder was covered by a layer of aluminum oxide and oxynitride. Binder burnout caused residual carbon to be adsorbed onto the AlN powder surface. A small

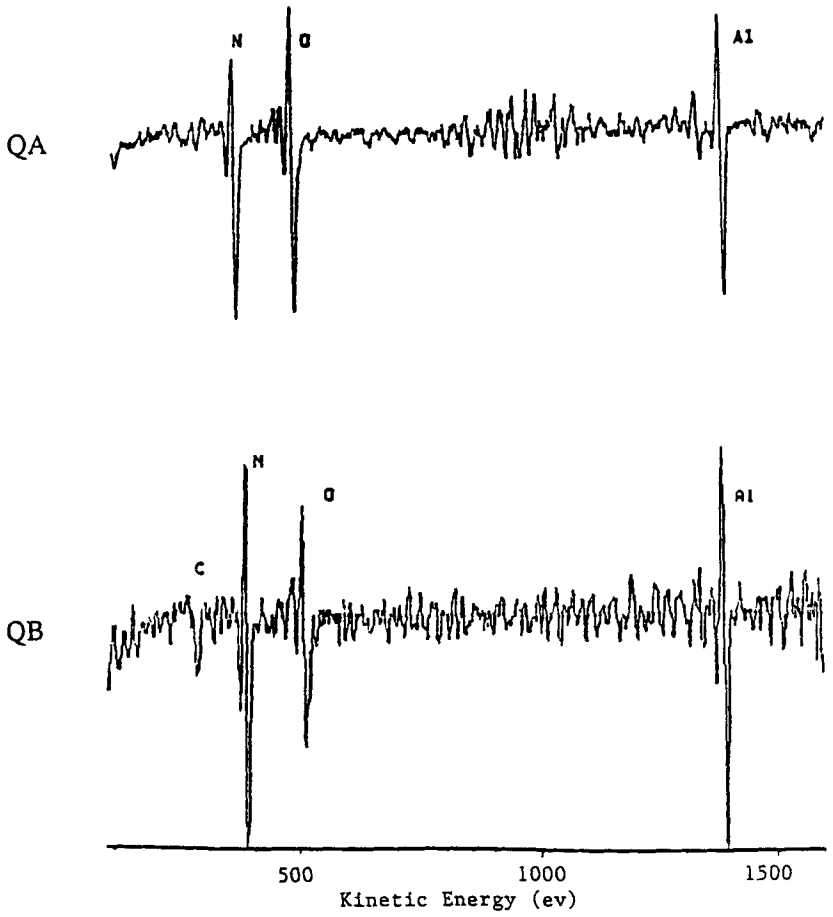

Fig. 7. AES spectra of AlN pellets.

portion of the residual carbon was bound to oxygen atoms at the AlN powder surface, and the majority of the carbon was amorphous graphitoid carbon which covered the AlN surface uniformly.

The C/O atomic ratio equal to 1.0 was apparently a threshold. When the C/O ratio was higher than this threshold, almost all the oxygen in the AlN sample was removed by a carbon-deoxidation reaction, and the AlN sample could not be sintered because of a lack of Al_2O_3 to form a liquid phase. In the region of C/O ratio less than 1.0, a higher C/O ratio was beneficial to thermal conductivity. The carbon-deoxidation reaction removed the oxygen impurities from the grain boundaries and changed the second phase from aluminum-rich to yttrium-rich. A corresponding increase in thermal conductivity was observed. The fact that the distribution of second-phase particles varied with different C/O ratios also could have affected the thermal conductivity. Nevertheless, there is a correlation between yttrium-rich phases and a low lattice oxygen content, and the low lattice oxygen content may be the more important factor contributing to a high thermal conductivity, as is widely believed.

Acknowledgment: Special thanks to Dr. D. A. Hensely for instruction and help in using the XPS and AES equipment.

References

[1]G. A. Slack, "Nonmetallic Crystals with High Thermal Conductivity," *J. Phys. Chem. Solids*, **34,** 321–35 (1973).

[2]Y. Kurokawa, K. Utsumi, and H. Takamizawa, "Development and Microstructural Characterization of High-Thermal-Conductivity Aluminum Nitride Ceramics," *J. Am. Ceram. Soc.*, **71** [7] (1988).

[3]S. F. Horvath, S. R. Witek, and M. P. Harmer, "Effects of Carbon and Calcium Oxide on the Sintering Behavior of Aluminum Nitride"; pp. 121–32 in Advances in Ceramics, Vol. 26, *Ceramic Substances and Packages for Electronic Application*. Edited by M. F. Yan, K. Niwa, H. M. O'Bryan, Jr., and W. S. Young. American Ceramic Society, Westerville, OH, 1989.

[4]K. Komeya, A. Tsuge, and H. Inose, "Sintered Bodies of Aluminum Nitride," U.S. Pat. No. 4 435 513, 1984.

[5]I. C. Huseby and C. F. Bobik, "High Thermal Conductivity Ceramic Body of Aluminum Nitride," U.S. Pat. No. 4 578 365, 1986.

[6]K. Schwetz, W. Grellneret, K. Hunold, M. Mohr, and A. Lipp, "'Dense Molded Bodies of Polycrystalline Aluminum Nitride and Process for Preparation without Use of Sintering Aids," U.S. Pat. No. 4 803 183, 1989.

[7]R. Lee, "Development of High Thermal Conductivity Aluminum Nitride Ceramic," *J. Am. Ceram. Soc.*, **74** [9] 2242–49 (1991).

[8]A. V. Virkar, T. B. Jackson, and R. A. Cutler, "Thermodynamic and Kinetic Effects of Oxygen Removal on the Thermal Conductivity of Aluminum Nitride," *J. Am. Ceram. Soc.*, **72** [11] 2031–42 (1989).

[9]G. A. Slack, R. A. Tanzilli, R. O. Pohl, and J. W. Vandersande, "The Intrinsic Thermal Conductivity of AlN," *J. Phys. Chem. Solids*, **48** [7] 641–47 (1987).

[10]L. Weisenbach, J. A. Ikeda, and Y. M. Chiang, "Distribution of Oxygen and Sintering Aids in Aluminum Nitride with High Thermal Conductivity"; see Ref. 3, pp. 133–44.

[11]K. Shinozaki, Y. Goto, K. Kasori, F. Ueno, K. Anzai, and A. Tsuge, "Thermal Conductivity and Microstructure of AlN Ceramics with Y_2O_3 Additives"; p. 175 in Proceedings of the 24th Symposium on Basic Science of Ceramics, Yogyo Kyokai, **1d13,** 175 (1986).

[12]J. H. Enloe, R. W. Rice, J. W. Lau, R. Kumar, and S. Y. Lee, "Microstructural Effects on the Thermal Conductivity of Polycrystalline Aluminum Nitride," *J. Am. Ceram. Soc.*, **74** [9] 2214–19 (1991).

[13]H. Yan, W. R. Cannon, and D. J. Shanefield, "Pyrolysis of Poly(vinyl Butyral): Interaction with Plasticizers and AlN Powder," *Mater. Res. Soc. Symp. Proc.*, **249,** 377–82 (1991).

[14]D. Whitman, "Mechanisms of Char Formation in Nitrogen Fired Thick Film Materials"; pp. 421–25 in Proceedings of the International Society for Hybrid Microelectronics. ISHM, Reston, VA, 1988.

[15]T. K. Hatwar and T. R. Pian, "Surface Studies of Aluminum Nitride Thin Films," *Mater. Res. Soc. Symp. Proc.*, **121,** 557–60 (1988).

[16]K. Ogata, Y. Andoh, and E. Kamijo, "Properties of Aluminum Nitride Films by Ion Beam and Vapor Deposition Method," *Nucl. Instrum. Methods Phys. Res.*, **B39,** 178–81 (1989).

[17]T. A. Carlson, *Photoelectron and Auger Spectroscopy*. Plenum Press, New York, 1975.

[18]E. Ponthieu, P. Grange, B. Delmon, L. Lonnoy, L. Leclercq, R. Bechara, and J. Grimblot, "Proposal of a Composition Model for Commercial AlN Powders," *J. Eur. Ceram. Soc.*, **8,** 233 (1991).

[19](a) G. H. Boe and E. Morrice, "The Gibbs Free Energy of Formation of Y_2O_3 in the Temperature Region 1000–1150 K," *Acta Chem. Scand., Ser. A*, **28** [9] 986–88 (1974). (b) D. R. Stull and H. Prophet, JANAF Thermochemical Tables, 2nd ed., NSRDS-NBS 37, 1971.

[20]M. Fujimoto and S. Ueda, "Effect of Annealing in CF_4 Gas Atmosphere on Thermal Conductivity of AlN Ceramics," *Nippon Seramikkusu Kyokai Gakujutsu Ronbunshi*, **96** [12] 1210–13 (1988).